JOURNAL OF GEOPHYSICAL RESEARCH, VOL. 99, NO. B7, PAGES 13,897–13,912, JULY 10, 1994

Constraints on Himalayan deformation inferred from vertical velocity fields in Nepal and Tibet

Michael Jackson[1] and Roger Bilham

Cooperative Institute for Research in the Environmental Sciences and Department of Geologic Sciences
University of Colorado, Boulder

Abstract. Spirit leveling data from the Nepal Himalaya between 1977 and 1990 indicate localized uplift at 2-3 mm/yr in the Lesser Himalaya with spatial wavelengths of 25-35 km and at 4-6 mm/yr in the Greater Himalaya with a wavelength of ≈40 km. Leveling data with significantly sparser spatial sampling in southern Tibet between 1959 and 1981 suggest that the Himalayan divide may be rising at a rate of 7.5±5.6 mm/yr relative to central Tibet. We use two-dimensional dislocation modeling methods to examine a number of structural models that yield vertical velocity fields similar to those observed. Although these models are structurally nonunique, dislocation models that satisfy the data require aseismic slip rates of 2-7 mm/yr on shallow dipping faults beneath the Lesser Himalaya and rates of 9-18 mm/yr on deep thrust faults dipping at ≈25°N near the Greater Himalaya. Unfortunately, the leveling data cannot constrain long-wavelength uplift (>100 km) across the Himalaya, and unequivocal estimates of aseismic slip in central Nepal are therefore not possible. In turn, the poor spatial density of leveling data in southern Tibet may inadequately sample the processes responsible for the uplift of the Greater Himalaya. Despite these shortcomings in the leveling data, the pattern of uplift is consistent with a crustal scale ramp near the Greater Himalaya linking shallow northward dipping thrust planes (3-6°) beneath the Lesser Himalaya and southern Tibet. Aseismic slip on the potential rupture surface of future great earthquakes beneath the Nepal Himalaya south of this ramp appears not to exceed 30% of the total convergence rate between India and southern Tibet resulting in an accumulating slip deficit of 13±8 mm/yr.

Introduction

The Tibetan Plateau constitutes the largest single region of high elevation on the Earth's surface. Despite its unique bulk and the unsurpassed elevations of the mountains bordering its southern edge [*Harrison et al.*, 1992], few geodetic measurements of the processes involved in its creation and sustenance exist. The reasons for this are partly found in its remoteness and partly in the difficulty in conducting height and distance measurements through the Himalaya. The Himalayan foothills formed a natural barrier to the northward growth of triangulation and leveling networks of the Survey of India. Although the primary surveys of unvisited Himalayan peaks were completed in the nineteenth century, it was not until the early part of this century that geodetic lines were carried beyond the Lesser Himalaya [*Gulatee*, 1954; *Dickey*, 1985]. A single trans-Himalayan survey connecting the Russian and Indian triangulation networks was undertaken in 1913 [*Mason*, 1914]. Space geodesy using the Global Positioning System (GPS) methods has recently been initiated in the region but will take several years to provide numerical data suitable for tectonic interpretation [*Jackson et al.*, 1991; *Jackson and Bilham*, 1994]. Leveling lines crossing the Himalaya were first measured in the last two decades along recently constructed highways in the Karakorum and Nepal. Of these two precision spirit leveling lines, only the survey in Nepal has been repeated.

Repeated leveling permits the rate of change of elevation to be determined as a function of location from some fixed datum, usually one of the bench marks in the leveling line. It is convenient to display the data from leveling lines from different remeasurement intervals by converting the observed changes in elevation to vertical velocities. We present data from vertical velocity fields observed in Nepal and Tibet in the past two decades and discuss their form and rate in the context of what they may reveal concerning the mechanics of the collision process in the Himalaya.

The rate of convergence between India and southern Tibet is believed to be between 10 and 25 mm/yr [*Molnar*, 1990]. In the absence of historical horizontal geodetic measurements crossing the range, the evidence for this rate of convergence is indirect. Relative plate motion reconstructions yield estimates for the convergence rate between India and Eurasia which, at the latitude of Nepal, indicate velocities of 55 mm/yr were the entire convergence rate concentrated across the Himalaya [*DeMets et al., 1990*]. More than half of this relative displacement, however, is absorbed by internal deformation and slip on faults in central Asia [*Molnar and Tapponnier*, 1975; *Molnar and Deng*, 1984; *Avouac and Tapponnier*, 1993]. The average rate of convergence based on the sum of seismic moment release this century yields a convergence rate of 17 mm/yr [*Molnar and Deng*, 1984], but this is clearly an insufficient time to obtain a precise rate. The rate of advance of sedimentary deposits toward India recorded in the sediments in the plains of India and Pakistan yields a conver-

[1] Also at Engineering-Science, Denver, CO.

Paper number 94JB00714.
0148-0227/94/94JB-00714$05.00

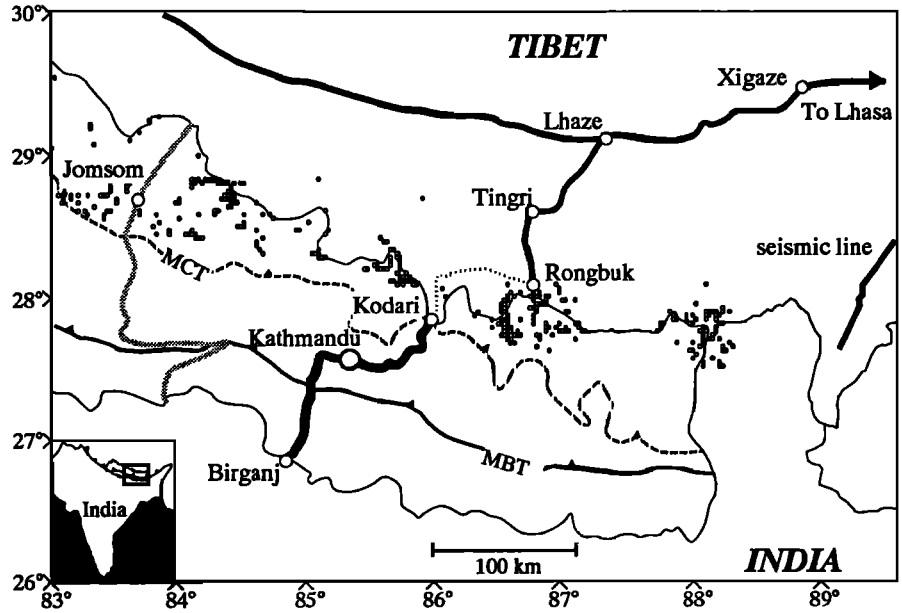

Figure 1. Locations of Nepal leveling route (solid line), the Project INDEPTH seismic line, and Kali Gandaki river (gray line). Chinese leveling network is shown as solid lines in Tibet. The link (dashed line) between Tingri and Kodari has been measured once only. Small open circles indicate Himalayan peaks > 6 km. MBT, Main Boundary Thrust; MCT, Main Central Thrust.

gence rate of approximately 10-20 mm/yr with a preferred rate of 15±5 mm/yr [*Lyon-Caen and Molnar*, 1985]. It is suspected that of the 15±5 mm/yr convergence rate between India and southern Tibet, 1-5 mm/yr may be absorbed on structures within the Himalaya [*Molnar*, 1987]. Uplift rates in the Himalaya have been estimated using fission track methods indicating local rates of 5 mm/yr during the past 0.7 my [*Zeitler*, 1985]. The local deformation of river terraces in the Nepal Himalaya is most intense in the Higher Himalaya and Lesser Himalaya suggesting that rates of uplift there may also approach 5 mm/yr [*Iwata*, 1987, *Molnar*, 1987].

Leveling networks on the Tibetan Plateau were remeasured by Peoples Republic of China (PRC) geodesists between 1959 and 1981 [*Zhang*, 1991], and a single line between the Tibetan border and the Indian border was measured twice between 1975 and 1991 by the Survey Department of His Majesty's Government (HMG) of Nepal (Figure 1). The Nepalese spirit leveling data are unique and invaluable in that they represent the only trans-Himalayan geodetic data available across a relatively narrow segment of the Himalayan arc.

In a previous analysis of the Nepalese leveling data, we estimated subsurface interseismic slip rates on an inferred subsurface thrust fault beneath the Siwalik foothills [*Jackson et al.*, 1992]. Bench mark coordinates and elevation change data for each recovered bench mark were unavailable to this previous study. Their incorporation in the present study resulted in an adjusted N-S uplift profile and improved estimates of vertical velocities and their uncertainties. In the present article, we examine the corrected velocity data supplemented by leveling data from the southern Tibetan Plateau [*Wang and Yang*, 1993] and new data on the subsurface geometry obtained from seismic reflection studies in Nepal and Tibet. Our goal in this study is to estimate the rate and distribution of interseismic convergence across the Himalaya. However, the non-unique interpretation of vertical motions in terms of their assumed causal horizontal motions presupposes an understanding of crustal structure and the subsurface mechanics at work within the Himalaya. The range of possible subsurface structural geometries and rates of deformation responsible for the Himalaya is large, and the surface deformation data available to us are perhaps more useful to reject untenable geometries than to identify ones that may be operative. We therefore limit ourselves to reviewing a subset of possible models. As an analysis tool we use two-dimensional elastic modeling methods and assume that it is possible to treat the collision zone as an elastic half-space with uniform elastic properties. This simplistic approach ignores the fact that the mechanics of an accretionary prism is moderated by gravitational as well as elastic and inelastic processes, that the topographic relief of the collision zone is severe, and that the scale of the collision process involves ductile and isostatic processes.

In the following treatment we first describe the nature and quality of the leveling data and discuss the geological and geometrical constraints on subsurface structures for the southern and northern segments of the leveling line. We then introduce several fault geometries which may be responsible for the observed vertical velocity fields in the southern and northern segments of the leveling line. We summarize the essential rates and geometries associated with these models and provide a lower bound for the India/Tibet convergence. We then compare a long-term slip rate model with the morphology of peaks in the Himalaya.

Leveling Data

The raw height data, provided by the HMG Survey Department of Nepal, are unadjusted by network links within Nepal (no network closures exist) or by links to India or China. The data available to this study consisted of bench mark coordinates and elevations for two epochs along five segments of the leveling line (Figure 2). Measurements on each of the five

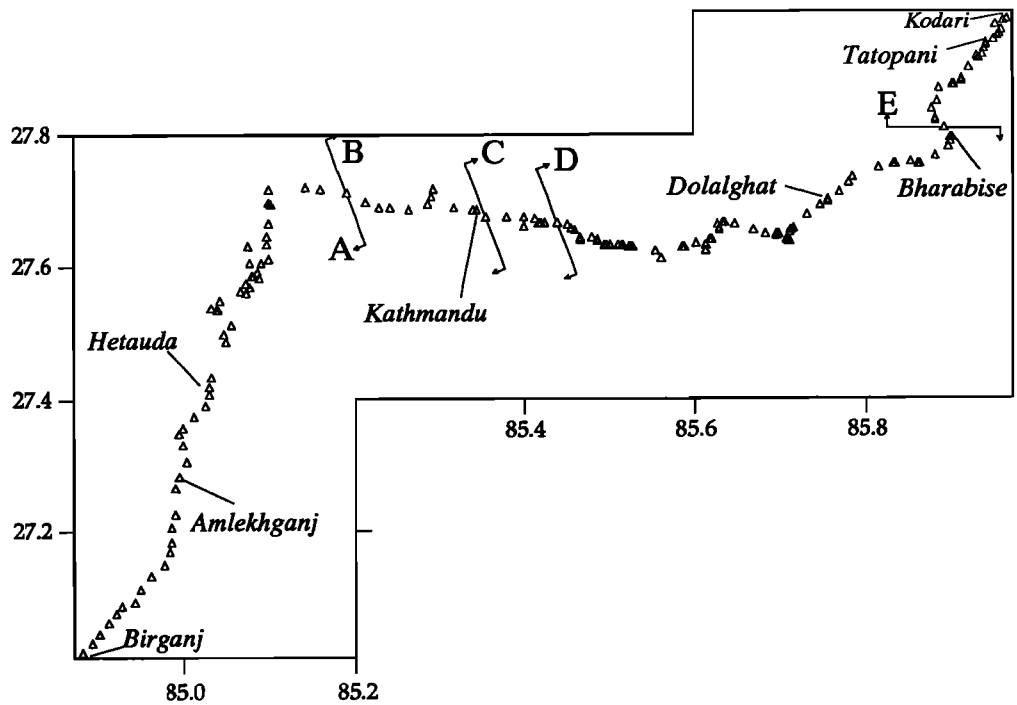

Figure 2. Map view of bench marks recovered in the 1975-1990 leveling surveys. Bars with arrows and large letters indicate segments of the line shown in Figure 3a measured at different times. Note the east-west segment traversing the Kathmandu Valley.

principal line segments took leveling parties 3-5 months each. While the cumulative along-line distance is ~350 km, the trans-Himalayan distance projected normal to the arc at 82°E is only 132 km. An east-west jog in the line through the Kathmandu Valley is responsible for most of the difference in these two distances, but a significant factor is the tortuous path encountered where the leveling line rises over the Mahabharat Range south of Kathmandu (Figure 2). Although the leveling line rises more than 2.5 km where it crosses the Mahabharat Range, relief near the Greater Himalaya is subdued as the level line follows first the Sun Kosi, and then the Bhote Kosi rivers to the Tibetan border at elevations between 0.8 and 1.6 km (see Figure 3a).

The leveling data south of Kathmandu were obtained over a 13-year interval (Figure 3). North of Kathmandu the line was remeasured at an interval of 7 years with the northernmost part of the line between Bharabise and Kodari remeasured after 2 years. The displacement data were normalized to vertical velocity by dividing by the appropriate measurement interval. These data are plotted in Figure 3b with the southernmost point near Birganj fixed to zero. However, because none of the bench marks are related to an absolute vertical datum during this interval of time, the vertical velocities are meaningful only in relation to each other and any arbitrary point could be held fixed in the data. Bench marks in the southern and northern segments were inspected for stability. Eight points from Figures 3a and 3b were removed because they were clearly unstable and showed subsidence exceeding several tens of centimeters. Despite the rough terrain, most of the bench marks are set in bedrock or cemented in concrete bridge abutments, often seated on bedrock. Bench marks in the Kathmandu Valley and in the Terai south of the Siwaliks are 1 m concrete pyramids set 0.5 m below the ground surface. Many bench marks in the Kathmandu valley appear to be unstable and show significant subsidence at rates of more than 5 mm/yr presumably related to groundwater withdrawal (Figure 3b).

Chinese leveling measurements join the Nepal leveling line at Kodari, yet this link has been measured only once in the segment that rises 3 km to the Tibetan Plateau (Figure 1). The closest releveled section of the Tibetan network consists of an approximately east-west line more than 100 km north of Kodari (Figure 4). This line meets a 400-km line that extends north through Lhasa to central Tibet. A measurement spur to the Rongbuk region north of Mount Everest, 100 km east of Kodari, was measured in 1966 and again in 1975-1977 in connection with measurements of the height of Mount Everest. The southernmost bench mark on this 80-km spur rose at a rate of approximately 1.5 mm/yr between 1966 and 1977 [*Wang and Yang*, 1993] resulting in an apparent tilt rate of 0.03 μrad/yr down to the north. The leveling data 300-500 km north of the Himalaya show no significant tilt of the Tibetan plateau.

Errors in the Leveling Data

Inspection of Figures 2 and 4 reveals that the quality and density of the leveling data from Nepal and Tibet differ substantially. In a previous analysis we showed that data from the southern and northern ends of the leveling line in Nepal are apparently free from slope dependent errors but that the line crossing the Mahabharat Range exhibits minor correlation between slope and line tilt and between elevation and elevation change [*Jackson et al.*, 1992]. According to Nepal first-order standards [*Shrestha*, 1988], random errors in the measurements have an uncertainty of 1.1 $\sqrt{L}$ mm, where L is the along-line length in kilometers. Thus, on the basis of random errors alone, the uncertainty in the height estimate between Birganj, at the Nepal-India border, and Kodari, on the Tibetan border is

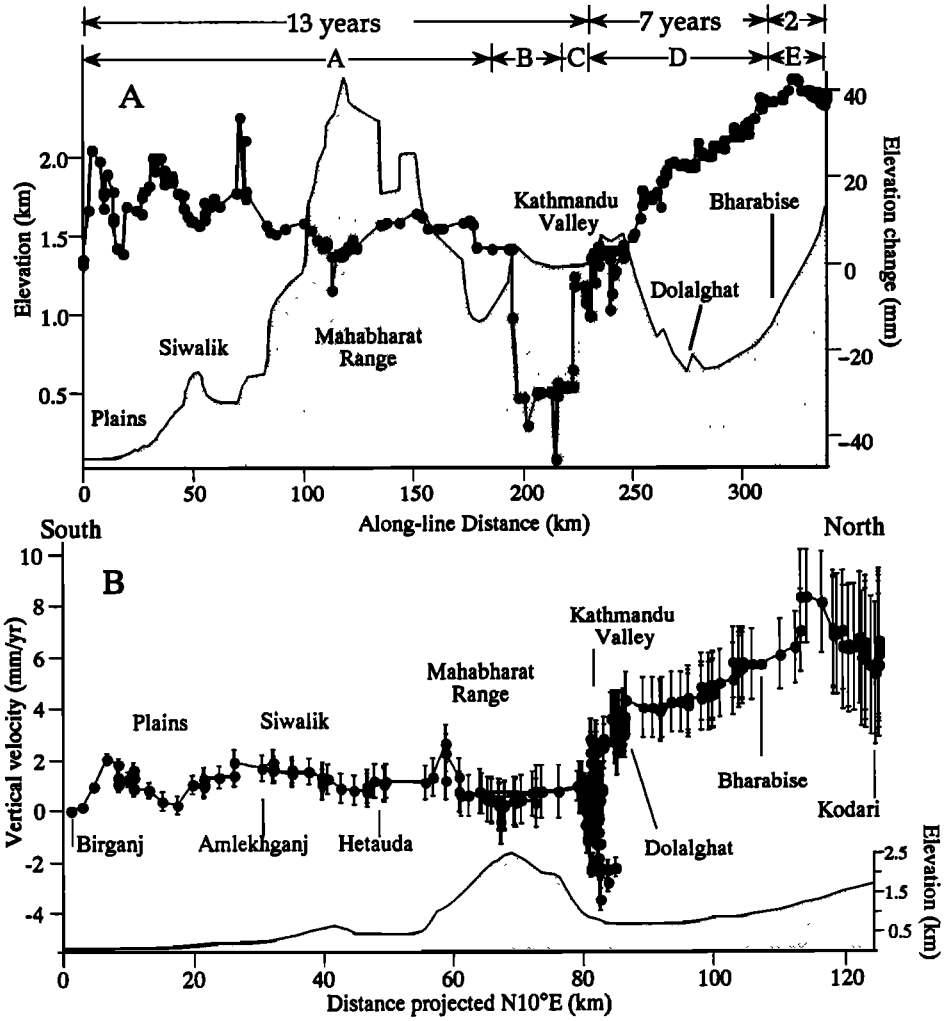

Figure 3. (a) Changes in elevation along the Nepal leveling line, with measurement intervals in segments A-E indicated. Shaded area corresponds to the topography along the leveling route. The zero vertical displacement and velocity datum is arbitrarily fixed to Birganj on the Indian border. (b) Vertical velocities and topography projected onto a line parallel to the inferred India-Asia convergence vector (N10°E). This projection considerably shortens the line where it crosses the Mahabharat Range and the Kathmandu Valley. Indicated random errors are initialized from the southern end of each leveling segment.

approximately 2 cm for each measurement epoch. Systematic errors can exceed 1 cm per vertical km adding perhaps an additional 2 cm uncertainty to long-wavelength estimates across the Mahabharat Range [e.g., *Holdahl*, 1981]. The cumulative differenced data are thus associated with along-line random errors between the Plains of India and the Tibetan border that grow to ±7 mm/yr (weighted to the measurement interval), with a possible additional systematic error of 3±3 mm/yr (weighted to measurement interval and measurement path) mostly associated with the southern half of the line. Thus the rate of uplift of the Greater Himalaya relative to the northern plains of India is 6.2±10 mm/yr providing a weak upper constraint on the growth of the range (Figure 3). In an absolute sense, even this estimate is flawed by uncertainties related to the stability of the southernmost bench mark whose elevation may have changed relative to tide gauges in the India Ocean during the past two decades.

Notwithstanding the poor signal-to-noise ratio of the long wavelength signal, vertical deformation with wavelengths of the order of 40 km in Nepal is relatively well constrained where the leveling line follows a path associated with subdued relief. The random error for these signals attains a maximum displacement uncertainty of ≈7 mm corresponding to a velocity uncertainty of less than ±0.5 mm/yr for bench marks measured after 13 years and ±1 mm/yr uncertainty for those measured after 7 years. The northernmost 16-km segment of the leveling line is associated with a maximum random velocity uncertainty of ±3 mm/yr between Bharabise and Kodari. In Figure 3b we illustrate the growth of random errors along the northern and southern uplift regions relative to a fixed point in each segment.

The Tibetan leveling network was first measured in 1959-1961 and remeasured in 1979-1981. The data are available as elevations and elevation changes of bench marks spaced at intervals of 20-70 km. The data have evidently undergone a network-adjustment in the PRC and Tibet, the details of these adjustments or of published tests for slope- and height-dependent errors for intermediate points are unavailable to us. We therefore estimate the accuracy of these data indirectly from a 1975 error analysis for the elevation of Mount Everest [*Gu*, 1976] in which the contribution from spirit leveling measurements and vertical triangulation

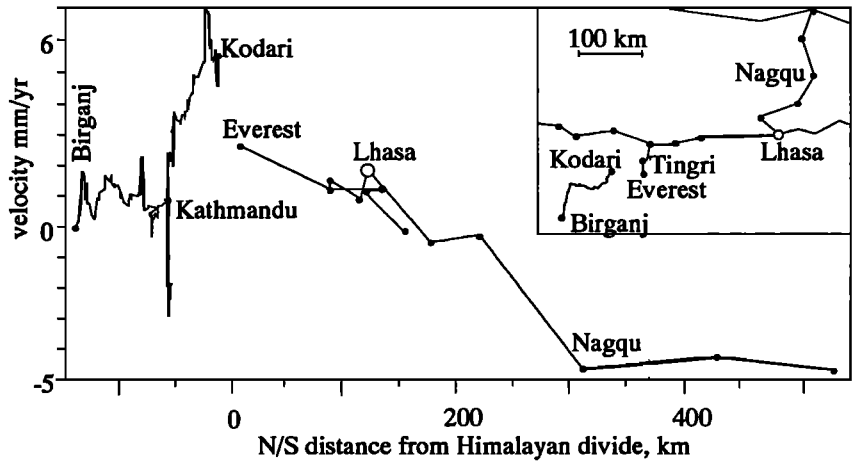

Figure 4. Leveling lines in Nepal and southern Tibet at the same scale and their published vertical velocity fields (1966-1990). The Nepal-Tibet velocity fields are derived for different time intervals and are referred to different, arbitrary datums. Inset shows map view locations of leveling bench marks in Tibet and the offset between the Nepal and Tibetan leveling lines. See text for discussion of errors.

measurements were assigned a combined uncertainty of 14 cm. If this uncertainty were entirely attributable to random errors, it would suggest that the propagating error for Tibetan data could be expressed as $k\sqrt{L}$ mm where k=2.4 and L=3400, the distance from the Gulf of Bohai in kilometers. However, it is possible that a 6-cm component of this uncertainty is associated with systematic errors associated with the ≈6 km rise in elevation of the end of the line near Mount Everest [*Bilham, 1988*]. In this case, k=1.4, which is approximately double the value obtained using the most favorable leveling procedures (first-order, class 1). The lower and upper error limits in the following calculations correspond to errors evaluated for k=1.4 and k=2.4, respectively. The vertical displacement uncertainty for the southernmost 80-km segment of the traverse is 12.5-21.5 mm for each measurement, resulting in a 1.6-2.8 mm/yr velocity uncertainty for the combined measurements over the 11-year interval. Application of the same reasoning to the contiguous line extending 500 km to the north yields a displacement uncertainty of 44-76 mm for the ≈1000 km along-line path and a remeasurement velocity uncertainty of 3.1-5.4 mm/yr for the 20-year interval. The northern 210 km of the line show no tilt in the two decades under investigation but the 230-km segment between Tingri and Nagqu indicates a relative vertical velocity of 6.5 mm/yr. The velocity uncertainty for this ≈800-km-long segment is 2.8-4.8 mm/yr, but this includes a ≈350-km east-west line segment that contributes substantially to the uncertainty. If Lhasa-Nagqu relative motions are considered, the relative velocity uncertainty reduces to 1.7-3.0 mm/yr. We compare these vertical rate estimates by converting them to tilt vectors and using the larger, more conservative, estimates for error growth. The apparent tilt rate of the southernmost 80 km is 19±35 nrad/yr down to the north, and the apparent tilt rate of the southern 300 km of the line is 28±19 nrad/yr down to the north. The first of these signals is not significant, although it is consistent with leveling farther to the north and with the tilt signal evident on the approximately east-west leveling line that follows the Indus Suture north of Kodari. Tilt between Tingri and Nagqu appears to be significant, although we note that our error estimates may incompletely characterize systematic errors in the data associated with local relief on the Tibetan Plateau. Height-dependent errors may exceed 10^{-6} L where L is the vertical distance in kilometers [*Holdahl*, 1981]. Bench marks vary in elevation by more than 1.4 km, and systematic differences between the two surveys equal to $3x10^{-6}$ L would generate 5-cm displacement errors corresponding to 5 mm/yr vertical velocity errors. Thus we believe that the apparent northward tilt of the southern Tibetan Plateau is marginally significant. Given the various uncertainties in assessing errors in the Tibetan data, we propose a conservative vertical velocity for points near the Himalayan divide relative to central Tibet of 7.5±5.6 mm/yr.

Interpretation of the Nepal Leveling Data

In this section we examine short-wavelength (5-40 km) uplift signals in the leveling data south and north of the Kathmandu Valley which emerge significantly above the noise in the data and appear to be associated with activity on local structures with geologic or morphologic surface expression. A second justification for treating the northern and southern halves of the leveling line in isolation is that these two segments are offset by a 100-km-along arc near the western end of the 1934 Bihar rupture where processes may vary along strike. In a later section we reconcile these local rates with the cumulative deformation of the range.

Southern Nepal

The southernmost uplift signal (Figure 3b) occurs between 0 and 20 km from the start of the leveling line, has maximum uplift velocities of 2± 0.5 mm/yr, and corresponds geographically to the alluvial plain north of the Indian border and south of the Himalayan Front. A broader uplift signal is located between 18-44 km, has a similar amplitude but lower significance (2±1 mm/yr), and may represent aseismic slip associated with the active thrust front of the Lesser Himalaya. A third uplift signal, located in the southern Mahabharat Range (45-65 km) north of the Main Dun Thrust (also called the Chaura-Marin Thrust by *Schelling* [1992]) and near the location of the Main Boundary Thrust, is not considered significant. Although the vertical velocity of the third feature (45-65 km) exceeds the random error (peak-to-trough uncertainties of 0.5 mm/yr), the leveling line climbs steep hill slopes over the 2-km-high Mahabharat range

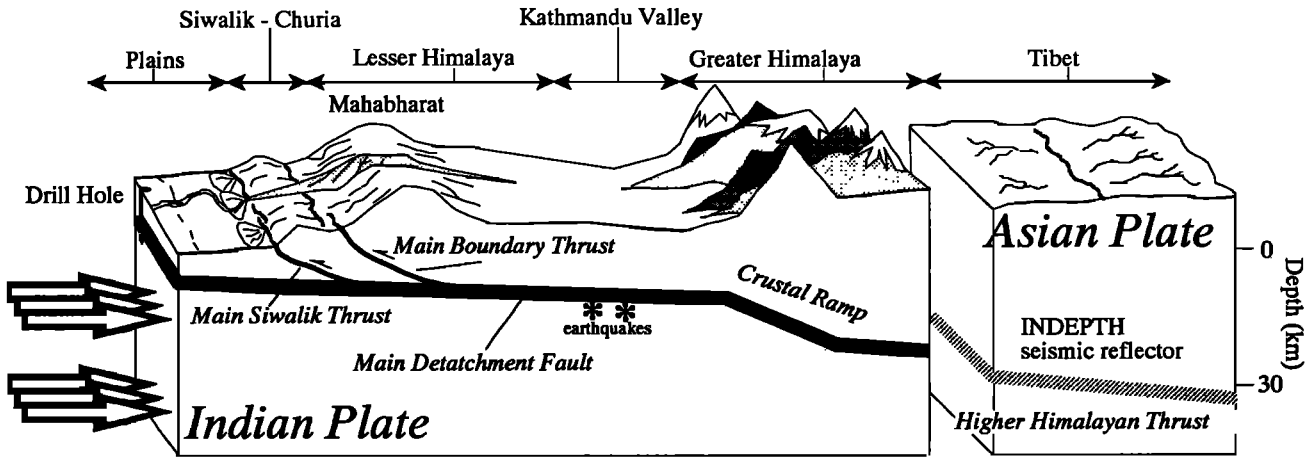

Figure 5. Sketch of elements of the Indo-Asia collision zone discussed in the text.

where systematic height-dependent errors may exceed 2 cm, thus more than doubling the possible uncertainty. We retain the two southernmost signals in models that follow and do not attempt to fit the northern feature.

Seeber and Armbruster [1981] suggest that great Himalayan earthquakes rupture a shallow dipping detachment (Main Detachment Fault) extending north beneath the Lesser Himalaya (Figure 5). The absence of recent great earthquakes, surface offsets, and depth estimates from microseismicity renders the precise subsurface geometry of underthrusting unknown. A number of constraints, however, can be placed on the fault geometry. On the basis of a single borehole beneath the Ganga Basin, *Mather and Kohli* [1964] estimate the upper surface of the Indian plate dips at 2-3° to the north beneath the Lesser Himalaya. Likewise, *Karunakaran and Ranga Roa* [1979] and *Sastri et al .* [1971] place the depth to the Indian Shield at ≈5 km based on the Raxaul exploration well in the Ganges Basin south of Birganj, Nepal. Detailed seismic reflection profiles undertaken by HMG Department of Mines and Geology suggest that the contact between the Tertiary and younger Siwalik sediments, representing a minimum depth to the Main Detachment Fault, dips gently (4-6°) to the north at a depth of 4.2-4.5 km beneath the plains of Nepal [*Bashyal*, 1990]. Interpretation of the seismic profiles indicates a sequence of northward dipping faults which appear continuous along strike (Nepal proprietary seismic profiles 31 and 31 extension, Figure 6). The seismic profiles are converted to a distance scale from the Nepal border using shot point coordinates from Doppler transit measurements located every five shot points. The two-way travel time is converted to depth using a seismic velocity profile obtained from nearby refraction and reflection data.

Profiles 31 and 31 extension follow the leveling line between Birganj and Hetauda (0-48 km). We interpret the southernmost structure identified in profile 31 as two fault segments (F1 and F2 in Figure 6) coinciding with the uplift feature located between 0 and 20 km. The shallower fault F1 dips 37° to the north, has a down dip length of 4.9 km, and offsets the contact between

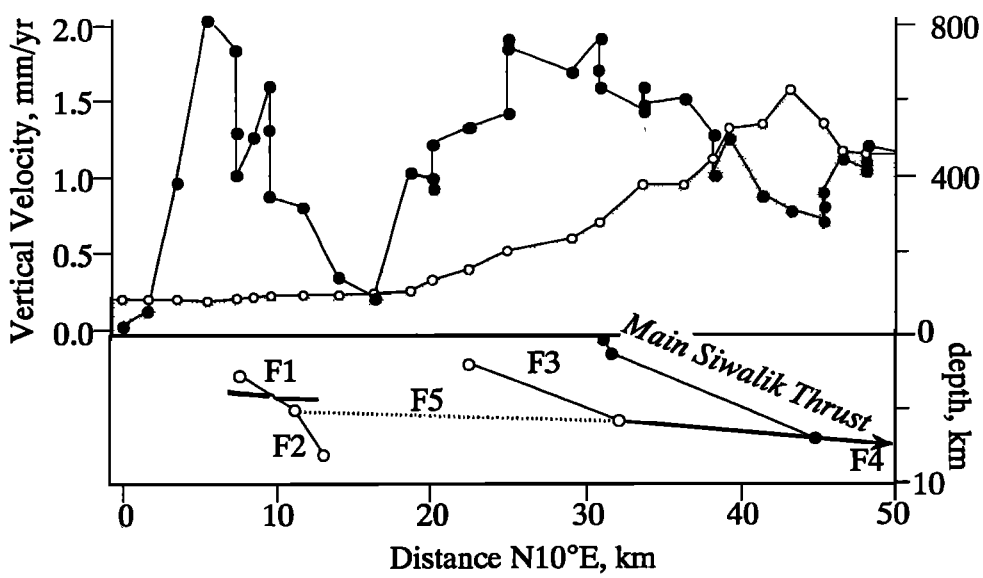

Figure 6. Relation between vertical velocity field and interpreted seismic profiles in South Nepal near border with India. Faults segments used in model inversions indicated by F1-F5. Dashed line F5 and solid line F4 are inferred detachment faults parallel to basement reflector. Topography along the leveling line shown as shading with open circles.

Siwalik and older basement rocks by 0.3 km in a normal sense. It is unknown whether this fault (F1) represents an emergent blind thrust, possibly reactivating a normal fault structure formed prior to or during the initial collision of India and Asia, or a creeping normal fault. Fault F1 is contiguous with a 3.9-km-long fault (F2) that dips 65° to the north and cuts deep into basement rocks (Figure 6). This fault can be traced along strike for at least 15 km to the west and 40 km to the east where seismic data suggest that its offset diminishes in amplitude. It is also evident that vertical offsets on the fault below the Siwalik vary downdip and appear to taper surfaceward. No evidence for upwarping of overlying sediments is detectable at the resolution of the seismic section, suggesting that if reverse faulting is occurring, it is relatively slow or relatively recent. Farther to the east, however, anticlinal doming over similar high-angle faults is evident in the seismic sections and suggests that they may now be acting as blind thrusts.

The northernmost fault identified on seismic profile 31 extension dips ≈35° at 0.1-2.0 km and shallows to 27° between 2 and 10 km depth (Figure 6). Its surface projection corresponds to the surface expression of the Main Siwalik Thrust (also called the Main Frontal Fault) that outcrops at the topographic front of the Himalaya near Amlekhganj. Few seismic profiles cross this fault, and although its downdepth geometry is conjectural, it is clearly a major feature that persists along strike. The Main Siwalik Thrust contact between Holocene alluvium and Middle Siwalik sediments is not exposed at the surface near Amlekhganj although a steep near-surface dip for a fault which shallows at depth can be inferred from steeply north dipping (80-65°) Middle Siwalik sediments at the mountain front which flatten to dips of 5-10° northward. The seismic profile 10 km south of the Main Siwalik Thrust is somewhat fragmented presumably by poor acoustic coupling of sources in the gravel fans fronting the Siwalik, but there is a suggestion of one or more shallow faults dipping to the north. Fault F3 in Figures 6 and 8 is interpreted as a footwall imbricate blind thrust propagating toward the surface from an inferred continuation of the Main Detachment Fault at depth. Although this fault has no visible surface manifestation, an active blind thrust with an extrapolated surface intersection 8 km south of the Main Siwalik Thrust is more consistent with the observed uplift data than is a signal generated by activity on the Main Siwalik Thrust.

Approximately 40 km east of the leveling line, *Schelling* [1992] infers that a gently north dipping basal detachment (Main Detachment Fault) underlies the Siwaliks and Lesser Himalaya at a depth of 6.9-8 km. He concludes that the Main Boundary Thrust, Main Dun Thrust, and the Main Siwalik Thrust are north dipping splay thrusts off this Main Detachment Fault that cut upward through the Siwalik sediments with no intervening thrust flats. Other constraints for the geometry of the active faults in the southern ranges are based on neotectonic analysis and the location and dip of surface faults. On the basis of a northward rotation of ≈20-kyr-old stream terraces, both *Nakata* [1989] and *Delcaillau* [1986] suggest that the dip of mapped frontal faults must shallow with depth.

The seismic profiles are uninformative concerning the existence of the inferred detachment fault beneath the Lesser Himalaya, and although several strong reflectors representing stratigraphic horizons exist, evidence for slip is conjectural. *Ni and Barazangi* [1984] show only one earthquake (depth 16±4 km) in the segment of the Nepal Himalaya close to the leveling line (≈ km 107, Figure 4) [also *Baranowski et al.*, 1984]. However, they offer a compilation of earthquake focal depths projected on a north-south line and suggest that the Main Detachment Fault lies at a depth of between 12 and 18 km just south of the Greater Himalaya [*Chen and Molnar*, 1990; *Ni and Barazangi*, 1984]. A surface drawn through an interpreted basement reflector 4.2-4.5 km beneath the plains of Nepal and passing through the average depth of the earthquakes [e.g., *Ni and Barazangi*, 1984, Figures 12 and 16] dips northward at ≈6° and lies at a depth of 15 km beneath the Lesser Himalaya at 107 km (Figure 5). This planar surface is shown as fault F4 in Figure 6 where the southward continuation (F5) is shown as the dashed line.

Deformation Models, Southern Nepal

The processes responsible for uplift are either aseismic or the seismicity is below the detection levels of the somewhat sparse Nepal seismic network (Figure 7). Deformation may be caused by elastic or inelastic processes that are conservative, implying no loss of mass, or nonconservative, involving a loss of mass from the system during deformation. We limit our search to models that are conservative and whose deformation is produced by some combination of slip on known or inferred faults. We further assume that the faults identified in the seismic profiles are adequately represented by a series of two-dimensional discontinuities in an elastic half-space. Although the fault geometry is known in some detail from seismic reflection data in southern Nepal, we are uncertain of what parts of the fault may be active or whether activity on faults extends beyond the segments visible on the somewhat low-resolution seismic sections available to us. Following a decision regarding the nature of the potentially active subsurface dislocation geometry, the observed vertical velocity field can be used to solve for fault slip rate using a standard linear least squares inversion [*Parker*, 1977; *Thatcher*, 1979; *Harris and Segall*, 1987]. The expression for the forward problem of vertical displacement due to slip on a buried dislocation in an elastic half space [cf. *Ward and Barrientos*, 1986; *Ellis and King*, 1991; *Stein et al.*, 1992] can be given in matrix form by

$$\mathbf{d} = \mathbf{G}\mathbf{s} \tag{1}$$

where $\mathbf{d}$ is a $n \times 1$ data vector of vertical velocity observations, $\mathbf{G}$ is a $n \times m$ matrix of Green's functions calculated using algorithms derived by *Okada* [1985, 1992], and $\mathbf{s}$ is a $m \times 1$ column vector whose components are the dislocation slip rate values. If we assume that the position and length of each fault segment are known from the seismic profiles, then (1) is a sequence of linear equations that can be inverted for the slip rate on each fault segment [cf. *Thatcher*, 1979; *Savage et al.*, 1979]. We amend the model to include a damping parameter λ^2 that allows a solution that minimizes both prediction error and solution length for the model parameters. Our least squares estimate of model parameters reduces to

$$s^{est} = \left[G^T G + \lambda^2 I\right]^{-1} G^T d \tag{2}$$

The advantage of the damped linear model is that in addition to including both prediction and solution error, repeated iterations to improve the data fits are unnecessary and the resulting slip rates are independent of the starting model. Disadvantages of this inversion method are that the specified dislocation geometry may not be representative of the spatially varying fault slip [*Segall and Harris*, 1986; *Langbein*, 1981]; the latter, however, can be

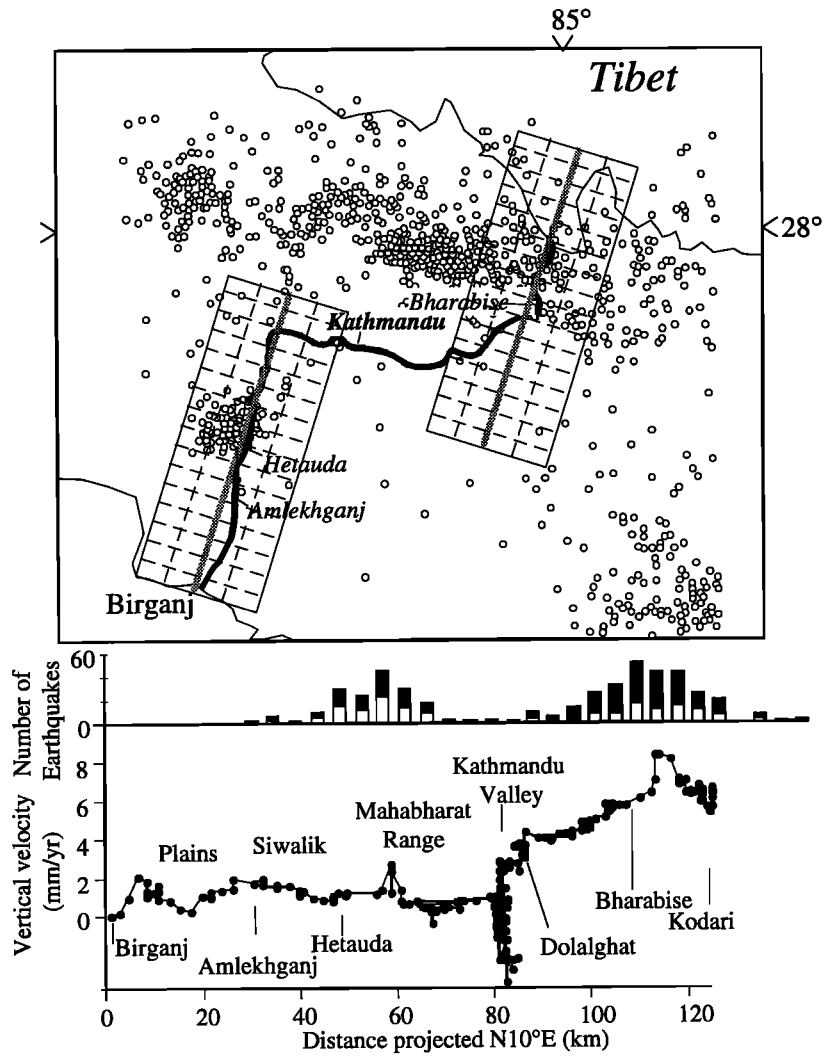

Figure 7. Microseismicity 1985-1990 (courtesy M. R. Pandey) near the HMG leveling line (thick solid line). The number of earthquakes within ±15 km and ±30 km of the leveling line (grids shown) are indicated by the white and black histograms respectively.

approximated by specifying apriori smoothness constraints on the slip distribution.

The procedure for inverting matrix equation (1) is uncomplicated where the number of vertical velocity data exceed the number of slip-rate unknowns [cf. *Jackson*, 1972; *Menke*, 1989]. For the over determined case (n > m), each model parameter is uniquely resolved (resolution matrix R = identity matrix I), and the inversion reduces to a simple weighted least squares or maximum likelihood problem. The leveling data have variable uncertainty which is often defined as the accumulating random error from an arbitrary bench mark [*Ward and Barrientos*, 1986; *Barrientos et al.*, 1987]. An alternative approach is to consider the random error that accumulates between adjacent points [*Vasco et al.*, 1990]. The velocity error for two epochs, a and b, between two bench marks i and i+1 is given by

$$\sigma_{i,i+1}^{a,b} = \sqrt{(\sigma_{i,i+1}^{a})^2 + (\sigma_{i,i+1}^{b})^2} \qquad (3)$$

where

$$\sigma_{i,i+1}^{a} = 1.1\sqrt{l_{i+1} - l_i}\,/t \qquad (4)$$

1.1 is a constant used for Nepal first-order leveling [*Shrestha*, 1988], l is the distance between the i and i+1 bench marks, and t is the time between measurement epochs a and b. For the inversion, the data vector d and the design matrix G are normalized by the random error between successive bench marks. Using weights inversely proportional to the random error between bench marks has the advantage of weighting stations that are closer together more than stations that are farther apart and does not assign arbitrary infinite weight to a station at the start of a leveling segment [cf. *Vasco et al.*, 1990]. For the actual inversion, we apply singular value decomposition techniques [*Lanczos*, 1961; *Lawson and Hanson*, 1974] to solve for the model parameters and the associated errors in the fitted parameters. For each inversion we vary the damping parameter λ^2 over a range of values (0-1X10^5) producing a trade-off curve (Figure 8) between variance reduction (prediction error) given by

$$V.R. = 100\left[1 - \left(\frac{\sum_{i=1}^{n}\left(d_i^{pre} - d_i^{obs}\right)^2}{\sum_{i=1}^{n}\left(d_i^{obs}\right)^2}\right)\right] \qquad (5)$$

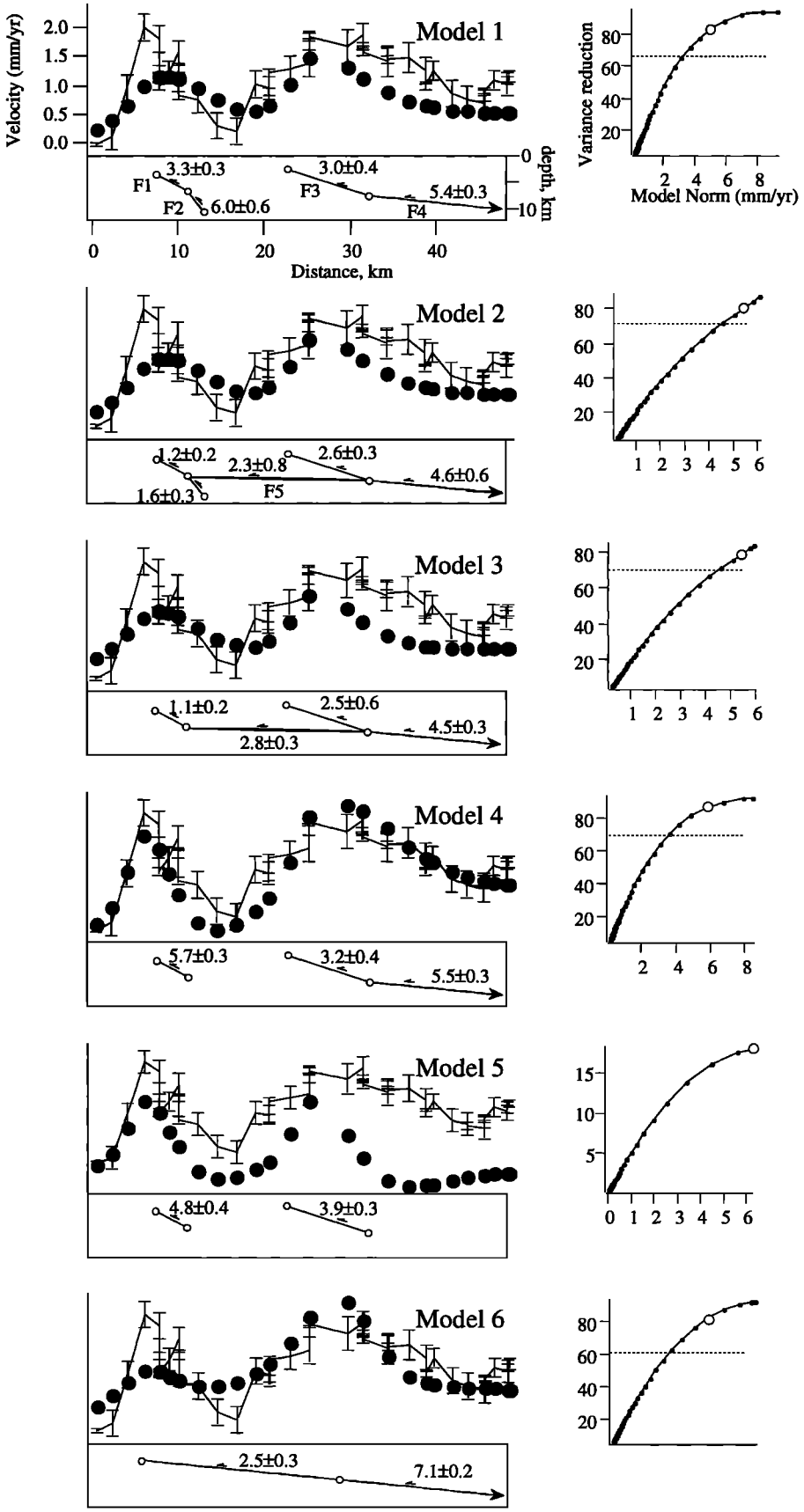

Figure 8. Observed (line with error bars) and synthetic (dots) vertical velocity fields for models with an optimum trade-off between model resolution and variance reduction (open dot on trade-off curve to right). The dislocation geometry in each model is fixed, and the slip on each segment was obtained using the inversion methods outlined in the text.

and model norm (model length) given by

$$M.N. = \sqrt{\sum_{i=1}^{m} s_i^2} \tag{6}$$

A very large value of λ^2 (small variance reduction, small model norm, Figure 8) will minimize the solution length at the expense of the prediction error, while a zero value of λ^2 (high variance reduction, high model norm, Figure 8) will minimize the prediction error but contains no apriori information regarding the model parameters. We choose a compromise solution by calculating the reduced χ^2 statistic at the 95% confidence level above which models cannot be differentiated (thin dashed line on trade-off curve) then present the slip rates for a model halfway between this boundary and the $\lambda^2 = 0$ solution (open dot on trade-off curve). Standard errors for the model parameters are estimated from

$$\sigma_j^s = \sqrt{\sum_{i=1}^{M} \left(\frac{V_{ji}}{w_i}\right)^2} \tag{7}$$

where V_{ji} are the columns of square of eigenvectors that span the model parameter space in the singular value decomposition and w_i are the singular values.

Using the fault geometry estimated from the seismic profiles, we invert for slip rate on the faults F1-F4 to yield slip rates on faults F1-F4 of 3.3 ± 0.3, 6.0 ± 0.6, 3.0 ± 0.4, and 5.4 ± 0.3 mm/yr, respectively (Figure 8, model 1). The resulting model parameters reproduce the observed interseismic velocity field reasonably well and are within the range of long term [*Schelling*, 1992] and short-term [*Molnar*, 1990] slip rate estimates. Quantitatively, the weighted rms misfit is given by

$$\left[\frac{1}{N-M}\sum_{i=1}^{N} r_i^2 \beta_i^2\right]^{1/2} \tag{8}$$

where the residual $r_i = o_i - c_i$ is the difference between the observed and calculated vertical velocity and β_i is a weighting factor given by

$$\beta_i = \frac{1/\sigma_i^2}{1/\overline{\sigma}^2} = \frac{1/\sigma_i^2}{1/N\sum(1/\sigma_i^2)} \tag{9}$$

The weighted rms misfit for the model is 0.4 mm/yr (Table 1), whereas the average standard error ($\overline{\sigma}$) for the observed vertical velocity data is 0.1 mm/yr and the weighted rms error

$$\left[\frac{1}{N}\sum_{i=1}^{N} \sigma_i^2\right]^{1/2} \tag{10}$$

is 0.4 mm/yr. The weighted rms model misfit is sufficiently close to the rms pure error to reject the possibility of lack of model fit.

To test the uniqueness of the slip values from model 1 and to explore other possible structural geometries beneath the Lesser Himalaya, fault elements are added and removed from the geom-

Table 1. Slip Rate of Inverted Models

Model Run	Fault Segment	Slip Rate, mm/yr	S.D.,m	wrms,mm /yr	Degrees of Freedom	χ^2	F Ratio
1	F1	3.3	0.3	0.35	39	26.2	1.0
	F2	6.0	0.6				
	F3	3.0	0.4				
	F4	5.4	0.3				
2	F1	1.2	0.2	0.57	38	38.3	0.7
	F2	1.6	0.3				
	F3	2.6	0.3				
	F4	4.6	0.6				
	F5	2.3	0.8				
3	F1	1.1	0.2	0.69	39	41.2	0.6
	F3	2.5	0.6				
	F4	4.3	0.3				
	F5	2.8	0.3				
4	F1	5.7	0.3	0.46	40	21.7	1.2
	F3	3.2	0.4				
	F5	5.5	0.3				
5	F1	4.8	0.4	1.57	41	169.8	0.2
	F3	3.9	0.3				
6	F4	7.1	0.2	0.37	41	28.3	0.9
	F5	2.5	0.3				

etry shown in Figure 8. In model 2 (Figure 8), a throughgoing detachment (F5), similar to that proposed for the Bagmati region 40 km east of the leveling line [*Schelling*, 1992], is added between fault segments F1 and F3 beneath the plains of Nepal. Inversion for model 2 parameters suggests a fit to the observed data similar to that in model 1 but with a substantial decrease in slip rate on the southernmost dislocations and an overall higher weighted rms (Figure 8 and Table 1). A slip rate of 2.3±0.8 mm/yr on a detachment beneath the plains of Nepal reduces the slip rate on the southernmost faults by nearly 40% but changes the slip beneath the Lesser Himalaya by less than 15%. We test the hypothesis that model 2 provides a significantly better fit than model 1 by comparing the variance of misfit between the two models. We construct the ratio $F = \chi^2_{v1}/\chi^2_{v2}$ where

$$\chi^2_v = 1/(N-M)\sum_{i=1}^{N}(o_i - c_i)^2/\sigma^2_{oi} \quad (11)$$

and σ^2_{oi} is the variance of the observed data [*Walpole and Meyers*, 1985]. We test the null hypothesis that the variance of the residuals of the two data sets are equal against the alternative hypothesis that the variances are significantly different. For F = 0.7, we cannot reject the null hypothesis at the 95% confidence level and conclude the two models are not significantly different.

Next, fault F2 is removed (model 3, Figure 8) simulating a locked fault below F1. Qualitatively, the fit to the observed vertical velocity field is similar to models 1 and 2. Quantitatively, the weighted rms misfit is greater than that for model 1 (Table 1) and has an F ratio of 0.6 which is marginally significant at the 95% confidence level suggesting model 1 provides a slightly better fit than model 3.

The geometry of model 3 is retained in the next iteration (model 4), but the basal detachment F5 between faults F1 and F3 is removed (i.e., the same geometry as model 1 but without the basement fault F2; Figure 8). The inversion for slip rates in model 4 provides a good fit to the observed velocity field with a weighted rms of 0.46. The F ratio for models 1 and 4 is 1.2, suggesting no significant difference between the two at the 95% confidence level. This model results in a higher slip rate estimate for fault F1 but has a similar slip rate beneath the Lesser Himalaya (F4 = 5.5±0.3 mm/yr) compared to previous models.

In model 5 (Figure 8) we eliminate all faults except F1 and F3. The resulting model parameters provide a poor fit to the observed data, and a comparison of the model variances yields an F ratio of 0.2, suggesting that model 1 provides a significantly better fit than model 5. In the final model we retain a single throughgoing detachment (faults F4 and F5, model 6) beneath the Lesser Himalaya and the plains of Nepal. The tip of fault F5 is terminated under the peak amplitude of the southernmost uplift feature, while the dislocation boundary between F4 and F5 is placed beneath the peak of the uplift feature between 18 and 44 km. Inversion results in a slip rate of 7.1 mm/yr beneath the Lesser Himalaya and a 2.5 mm/yr slip rate beneath the plains. An F ratio of 0.9 suggests there is no significant difference between models 1 and 6 at the 95% confidence level.

The slip rate estimates indicated in the models minimize the sum of the squares of the residuals between the observed and synthetic vertical velocity fields given the fixed fault geometry and uniform slip on the fault segments indicated. Models 3 and 5 are rejected because of their poor fit to the data (Table 1) but models 1, 2, 4, and 6 yield equally valid interpretations of the data. One conclusion from these models is that although an active subhorizontal fault extending northward beneath the Siwalik is common to the models, we are unsure if activity continues south of its intersection forward of the Main Siwalik Thrust. The slip required on the southward dipping detachment is 4.5-7.1 mm/yr, a rate that is a substantial fraction (25-30%) of the inferred convergence rate across the Himalaya. This aseismic slip occurs presumably on, or close to, the rupture surface visited by great Himalayan earthquakes suggesting that interseismic processes locally either delay rupture or reduce coseismic slip.

Models 1 and 2 require reverse slip on the steeply dipping (60°) fault (F1 and F2) that offsets basement rocks under the plains of Nepal. This represents a reversal of geologic slip in that the fault clearly offsets sediments in a normal sense by up to 300 m. The angular intersection between F1 and F2 evident in seismic sections may signify that fault F1 has been rotated to a shallower dip by basal tractions and surface shear associated with southward propagation of the Himalayan front. In this view, the intersection of F1 and F2 is perhaps related to the incipient formation of a detachment thrust.

Northern Nepal

The leveling line crosses the Kathmandu Valley in an approximately east-west direction and climbs out of this alluvial valley before descending to the river valleys of the Sun Kosi and Bhote Kosi which it follows to the Tibetan border at Kodari (Figures 1 and 2). The maximum vertical velocity observed near the Tibetan border is 6±3 mm/yr (Figure 3b) on a 40-km wavelength uplift feature with a maximum flank tilt rate of 0.25 μrad/yr centered ±10 km from the location of maximum uplift rate. These observations, however, have the largest uncertainties because they were surveyed after the shortest time interval. The 40-km wavelength uplift feature is centered roughly over the location of a mapped anticline that has deformed the Main Central Thrust [*Gansser*, 1981; *Stocklin and Bhattari*, 1980] exposed at the northern end of the line near the border with Tibet. An offset in the leveling data suggests that of surface faulting occurs near the summit of the anticline but does not correspond to any known fault, and the debris-covered floor of the valley traversed by the leveling line at this point provides no clear evidence for recent faulting. In elastic models that follow we treat this apparent offset in the data as noise and define the growth of errors relative to a bench mark near Bharabise which we hold fixed. The 7.5±5.6 mm/yr vertical velocity estimate of the southern edge for the Tibetan Plateau relative to central Tibet provides a weak constraint for the uplift rate north of Kodari.

The geometry of the interface between India and Asia near the Tibetan border is not well defined by microseismicity and detailed seismic reflection profiles are unavailable to guide our selection of suitable subsurface geometries for potentially active faults. Focal mechanism solutions, gravity data, and estimates of flexural rigidity led *Seeber et al.* [1981], *Ni and Barazangi* [1984], and *Lyon-Caen and Molnar* [1985] to infer that the dip of the basal thrust is shallow beneath central Nepal (≈2-6°) and steepens in the north (≈15°) as it dips beneath the line of Himalayan peaks marking the edge of the Tibetan Plateau (Figure 5). The proposed crustal scale ramp feature is consistent with gravity data [*Lyon-Caen and Molnar*, 1983] and with the varying elevation of ancient river terraces along the Kali Gandaki river to the west of the leveling line [*Iwata et al.*, 1984; *Molnar*, 1987, 1988]. Likewise, the persistence of the ramp through time is used to explain the location and elevation of the high Himalayan peaks. The 40-km-long uplift feature found in the Greater

Himalaya is near the location of this inferred crustal scale ramp and corresponds to the broad anticline that has deformed the presumed inactive Main Central Thrust.

The geometry and depth of the ramp is somewhat conjectural, although its existence is suggested from balanced geologic cross-sections in northeast Nepal [*Schelling and Arita*, 1991]. A recent seismic reflection profile in southernmost Tibet reveals a 6°, northward dipping, 28-40 km deep reflector (the Main Himalayan Thrust) that may represent the northward continuation of the interface between India and Asia [*Nelson et al.*, 1992; *Zhao et al.*, 1993]. Gravity data [*Lyon-Caen and Molnar*, 1983, 1985] requires that the Main Detachment Thrust dip northward at 3-5° beneath the Lesser Himalaya and attain a depth of 15±5 km as it approaches the Greater Himalaya where it steepens in dip to roughly 15°. Earthquake focal depths [*Baranowski et al.*, 1984; *Ni and Barazangi*, 1985; *Chen and Molnar*, 1990] and focal mechanisms lend support to these geometric features. Microseismicity in the Greater Himalaya between 1985 and 1990 indicates a 40-km along-arc region of diffuse seismicity near Bharabise (Figure 7). Although some researchers interpret sparse seismic reflection data from the region in terms of large-scale southward dipping interfaces beneath the Himalaya [*Lépine et al.*, 1984; *Hirn and Sapin*, 1984], *Molnar* [1988] argues for an alternative interpretation of these data consistent with a northerly dipping interface. Thus the available data suggest that the interface between India and Asia dips northward at 3-5° south of the Greater Himalaya and 6° north of the Greater Himalaya with the two surfaces offset 5-10 km by a crustal scale ramp dipping approximately 15° to the north.

Deformation Models, Greater Himalaya

Several elastic dislocation models can emulate the amplitude, approximate symmetry and 40-km wavelength of the observed vertical velocity field in northern Nepal. However, two distinct categories of subsurface structure can be invoked: (1) north dipping throughgoing detachment faults (including the ramp structure discussed above) or faults terminating beneath or near the center of the uplift, or (2) vertical regions of contraction centered beneath the region of uplift. Subsurface volume contraction is associated with metamorphic processes related to dewatering and the replacement of minerals by denser minerals and by mass removal by pressure solution. Calculations indicate that the observed vertical velocity field can be generated by a >4-km-high, vertical line of contraction no shallower than 8 km depth or by distributed convergence at shallower depths. Numerous hot springs occur in northern Nepal near the Main Central Thrust in the Greater Himalaya and the Main Boundary Thrust in the Lesser Himalaya [*Bhattarai*, 1980]. Tatopani, meaning hot water in Nepalese, is a common village name. Although the location of these springs is consistent with our suggested contraction mechanism, *Bhattarai* [1980] argues for a nonmetamorphic origin for their waters based on mineral composition. Moreover, the cumulative mass effusion rate from the sum of dissolved and suspended matter is approximately an order of magnitude too low to account for the observed deformation rates. Thus although metamorphic processes constitute an appealing mechanism in deforming the accretionary prism, currently available data do not support a detailed analysis of contraction models.

In the following dislocation models we fix the geometry of a Main Detachment Fault south of the Greater Himalaya to dip 6° to the north at a 15.5 km depth 107 km north of the Indian border (F4 in Figure 9). We are guided in the selection of fault geometries by the depth of earthquake focal mechanisms reported by *Seeber et al.* [1981] and *Ni and Barazangi* [1984] and by structural interpretations by *Schelling* [1992] and *Schelling and Arita*

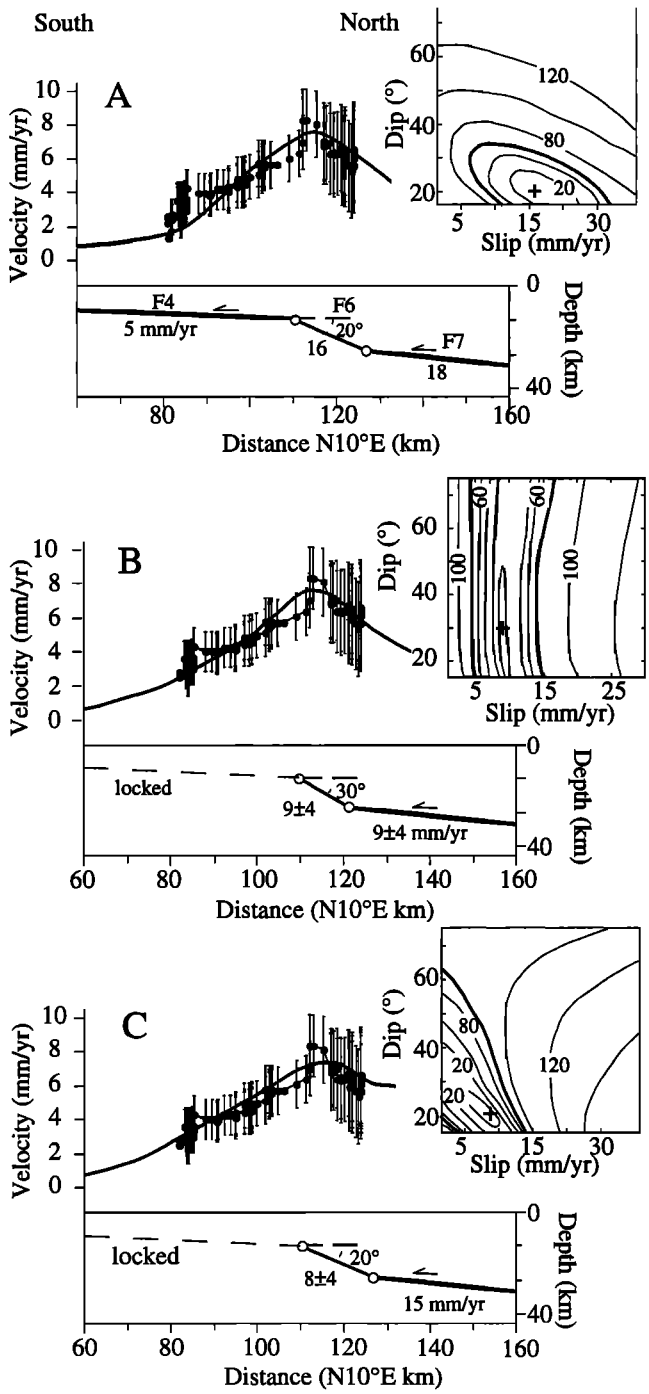

Figure 9. Deformation models for northern Nepal. (a) Slip on a shallow detachment (F4) is fixed at 5 mm/yr and slip on F6 and F7 varied to best fit (solid line) the observed data (dots with error bars). In Figures 9b and 9c F4 is locked. (b) uniform slip is imposed on F6 and F7. (c) Slip beneath Tibet is fixed at 15 mm/yr. The contours (chi square misfit) in each box indicate the trade-off between ramp dip and slip rate. The geometry of the best fitting solution (cross in contour diagram) shown beneath the observed and synthetic uplift data.

[1991]. We assume that the Main Himalayan Thrust of *Zhao et al.* [1993] and *Nelson et al.* [1992] as determined from the Project INDEPTH profile (F7 in Figure 9) is located at 29 km depth, 20 km north of Kodari. We link these two planar surfaces with a ramp thrust beneath the Greater Himalaya (F6 in Figure 9) whose dip, position and slip rate we estimate by forward modeling. We compare the observed vertical velocity field with a synthetic field generated from various assigned values of slip rate and ramp dip using the boundary element code developed by *Gomberg and Ellis* [this issue] and methodologies used by *King et al.* [1988] and *Bilham and King* [1989]. By segmenting the structure as a series of contiguous planar dislocations with variable dip and slip rate, we are able to test ramp features with approximately smooth curvature, but we find that the deformation data are inadequate to distinguish between linear or curved ramps. For the planar dislocations we find that the position of the ramp thrust is well determined by the peak in the vertical velocity field but that a trade-off occurs between ramp dip and ramp slip rate. To determine optimum combinations of these two parameters, we change the dip (18-70°) and slip rate (0.1-30 mm/yr) of the ramp and compare the resulting synthetic velocity field to the observed data as contour plots of χ^2 misfit as defined above (Figure 9). Preferred models are those that minimize χ^2 statistic between model results and observations [e.g., *Barrientos et al., 1987*]. The significance of the best fitting model is computed using the F ratio [*Walpole and Meyers*, 1985] between the model with the minimum χ^2 and alternative models. Model parameters yielding results within the 95%-confidence-contour equally explain the observed vertical velocity field.

In Figure 9a we fit the data from northern Nepal using a slip rate of 5 mm/yr for the detachment F4 determined from model 3 (Figure 8). For the error analysis, the data points in the ~80-km-long east-west jog in the leveling line passing through the Kathmandu Valley are removed to prevent these data from biasing estimates of quality of fit. The best fitting model allows continuous slip of 18± 2 mm/yr on a 6°, north dipping detachment beneath Tibet linked to a 20^{+6}_{-2} northward dipping ramp slipping at 10±4 mm/yr.

We next assume that no slip occurs in the interseismic period on the inferred rupture zone of great earthquakes south of the Greater Himalaya and generate an alternative suite of models for ramp geometry and slip rate (Figures 9b and 9c). In Figure 9b we assume uniform slip beneath southern Tibet and on the ramp thrust. Although the dip of the ramp thrust is poorly constrained in these models, the estimated convergence rate of 9±4 mm/yr between India and southern Tibet is reasonably well constrained, yet this rate is significantly lower than that predicted by other studies [*DeMets et al.*, 1990; *Lyon-Caen and Molnar*, 1985]. In Figure 9c we again assume no aseismic slip beneath central Nepal, but we fix the convergence rate beneath Tibet at 15 mm/yr [*Molnar*, 1990; *Lyon-Caen and Molnar*, 1985] to estimate the required dip and slip rate on a crustal ramp consistent with the observed surface deformation. Again the northward dip of the ramp is not well constrained (25^{+35}_{-10}) but slip on the ramp is reasonably well determined at 8±4 mm/yr. Deformation data north of the Greater Himalaya would significantly decrease the uncertainties in these estimates.

Discussion

The 18 mm/yr convergence rate between India and southern Tibet determined in Figure 9a is consistent with previous studies [*Molnar*, 1990]. This model, however, requires aseismic slip of 5 mm/yr beneath the Lesser Himalaya, a zone where historically great thrust earthquakes have occurred [*Pandey and Molnar*, 1988]. In the models in Figures 9b and 9c we lock this inferred seismic rupture zone and require somewhat lower convergence rates between India and Tibet. The most reasonable model is perhaps that of Figure 9c where a 15 mm/yr convergence rate is consistent with the leveling data. The recurrence interval for great earthquakes in the Nepal Himalaya depends on the rate of accumulation of a slip deficit south of the Greater Himalaya, which in turn depends both on the rate of India-Tibet convergence and the rate at which this convergence is released locally by aseismic slip. In the models shown in Figure 9a, 9b, and 9c the rate of accumulation of this deficit is 13, 9, and 15 mm/yr respectively.

The existence of aseismic slip beneath central Nepal is not required by the leveling data, yet we may exclude the possibility that the entire convergence signal is dissipated as aseismic slip. In Figure 10 we display the trans-Nepal leveling line with its cumulative error growth from the Indian border (in Figure 2 we

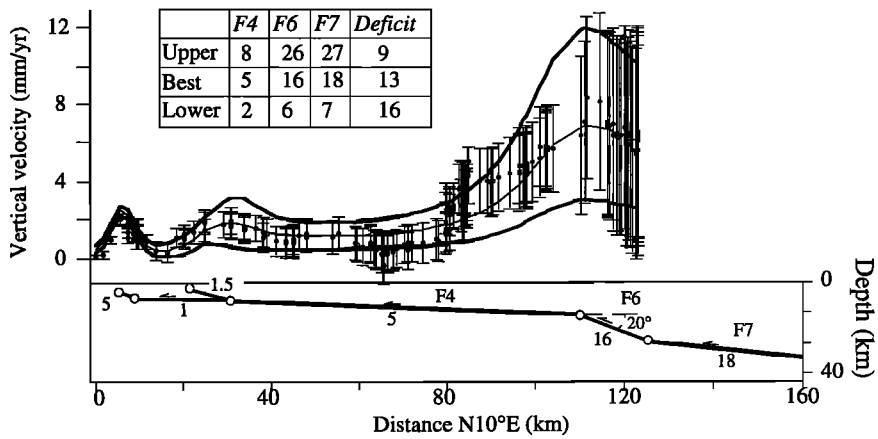

Figure 10. Nepal leveling line with cumulative error (circles and ±1 sigma error bars) growing from Indian border. The best fitting forward model is shown (thin solid line) with the model that best fit the upper and lower one sigma deviation envelope (thick lines). Inset table shows fault slip rates for ±1 sigma and best fitting model and the slip deficit accumulating beneath central Nepal.

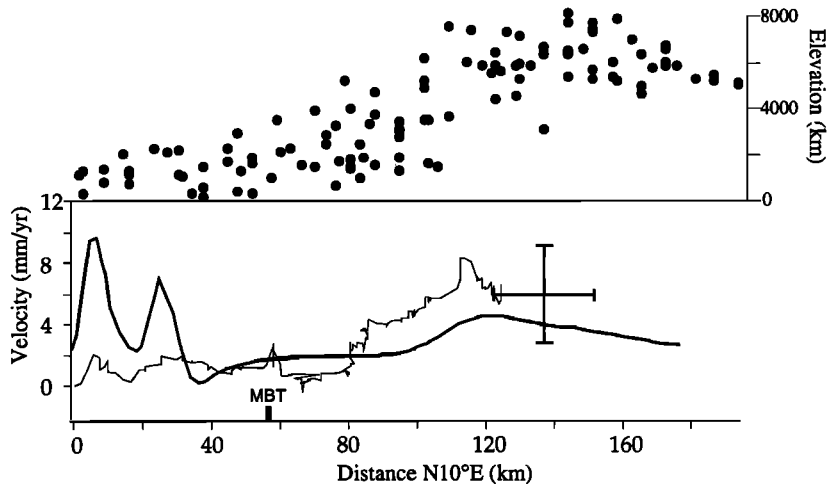

Figure 11. Solid circles are mountain peaks elevations ±50 km from leveling line between the plains of India and the Tibetan plateau. Vertical velocity data from spirit leveling in Nepal (thin solid line) and Tibet (large cross) superimposed on the surface uplift rate resulting from uniform slip of 18 mm/yr on the geometry shown in Figure 10 and corresponding to the sum of many coseismic and interseismic cycles.

displayed error growth from the start of each segment). Forward models fit to the upper and lower limits of the 1 sigma deviation envelope centered on the data yield slip rates beneath central Nepal of 8 and 2 mm/yr, respectively, with corresponding India/Tibet slip rates of 29 and 7.2 mm/yr respectively. These extreme value models are inconsistent with geologic estimates of convergence, yet they reveal that a slip deficit will develop beneath central Nepal at rates of at least 5 mm/yr and perhaps as high as 21 mm/yr. GPS data from Nepal between 1990 and 1992 [*Jackson and Bilham*, 1994] do not support rates significantly greater than 20 mm/yr. A slip deficit accumulating at 13-15 mm/yr in the region of the 1934 Bihar earthquake (~6 m slip) would have a renewal time of ~500 years. If we admit to the 5-21 mm/yr estimate permitted by the leveling data, then the renewal time for great earthquakes with 6 m of coseismic slip is 250-1000 years.

Over a complete earthquake cycle, the net vertical deformation field is represented by the sum of interseismic and coseismic deformation. We use the heights of peaks within ± 50 km from the leveling line as a proxy for the cumulative uplift signal. The position and height of the mountain peaks depend on the competing processes of erosion and vertical movements due to isostatic compensation and tectonic uplift. Because long-period vertical velocities recorded by the peaks include process other than the elastic deformation fields we have investigated, we should not anticipate close agreement between morphologic markers and deformation associated with seismic cycle. Yet we may consider deformation during the seismic cycle as the driving signal to which isostasy, erosion, and inelastic processes respond.

Assuming that great earthquakes rupture those segments of our models that are deficient in slip during the current aseismic stage of the earthquake cycle, the tectonic deformation field driving the morphology of the Himalaya can be estimated by assigning uniform slip of 18 mm/yr on all dislocations shown in Figure 10. If we do this, we find that uplift occurs forward of the high Himalayan peaks (Figures 1 and 11). River terrace data described by *Iwata et al*. [1984] along the Kali Gandaki also suggest that uplift is occurring north of the leveling line; however, the along-arc registration of the terrace and leveling data is problematic. Thus, either different processes are responsible for the concordance of the high peaks, or their southern flanks have been eroded, or additional structures are activated during the coseismic stage of the earthquake cycle. If we were to admit that thickening of the accretionary wedge is currently occurring by steady state southward reduction of slip on a basal detachment, the peak uplift region would be driven farther south of the maximum shown in Figure 11.

The mean uplift signal for many earthquake cycles across Nepal is 3.8 mm/yr. This includes the region of significant deformation near the southern end of the accretionary wedge, the details of which will differ depending on the activation of different combinations of shallow faults. Note that this mean uplift rate is almost double the rate associated with the forward motion of a 6° tapered wedge at 18 mm/yr. If we assume that erosion and uplift are equal and that the uplift rate for Nepal is applied to the entire range (100x2000 km^2), then the mean erosion rate would be 0.76 km^3/yr. The mass removal rate is equivalent 8280 t/km^2/yr using a mean density of 2.3 g/cm^3. These estimates are within an order of magnitude of erosion rate estimates based on sediment transport through the Ganges [*Milliman and Syvitski*, 1992] and volume accumulation rates for the Bengal fan [*Copeland and Harrison*, 1990].

Conclusions

Leveling data across Nepal provide valuable insight regarding the deformation processes responsible for the formation of the Himalaya. We propose a range of subsurface structures which may be responsible for the observed vertical velocity field using the simplifying assumption that two-dimensional elastic processes account for the short term deformation in the Himalaya. Presumably, these processes acting over long periods drive inelastic mechanisms resulting in permanent deformation. In addition to assuming dislocation slip is a mechanism for creating surface deformation fields, we suggest that subsurface volume contraction (pressure solution or metamorphism) may also contribute to local uplift features. From the vertical deformation field alone we are unable to distinguish between the models we present although some appear more plausible than others.

In southern Nepal we are guided in our selection of possible

deformation models by the availability of seismic reflection data near the leveling line that reveal several candidate subsurface faults which, if slipping at rates of 2-7 mm/yr, could be responsible for the observed deformation. A common feature of these models is a requirement for 4.5-7 mm/yr of slip on a shallow detachment fault extending northward beneath the Lesser Himalaya. This suggests that locally, the rupture surface of great detachment earthquakes may be creeping, hence releasing some of the slip available for seismic rupture.

In northern Nepal, higher rates of uplift over a broader region require slip on a northward dipping thrust fault at depth. We are guided in the selection of the downdip depth of this thrust fault by the recent finding of a shallow dipping reflector beneath southern Tibet that may represent the upper surface of the Indian plate. Slip rates of 9-18 mm/yr beneath southern Tibet and on this ramp thrust fault satisfy the leveling data, the lower rates being associated with a locked detachment surface beneath central Nepal. The location, dip, and scale of this thrust fault are similar to the crustal scale ramp invoked to explain gravity data and some seismic data near the Greater Himalaya. It is tempting to conclude that the leveling data confirm the existence of this ramp thrust; however, because the leveling data diminish in accuracy toward the border with Tibet and are sparse north of the Tibetan border, it is possible that the thrust fault we are modeling may lie forward of the crustal scale ramp invoked to explain the growth of the high peaks bordering southern Tibet. This conclusion is also suggested by river terrace data extending into the Mustang region of Nepal 200 km to the west.

Because of the unknown contribution from systematic height dependent errors and the known uncertainties from random errors in the leveling data, the long-wavelength uplift signal across the Himalaya in this interseismic period is poorly determined. Upper limits on the signal are estimated to be 6±5 mm/yr. If we are to reconcile the slip rates on structures determined for southern and northern Nepal, higher rates of uplift would require slip of ~8 mm/yr beneath central Nepal whereas lower rates permit an essentially locked zone beneath central Nepal. Thus, although the leveling data do not permit a complete understanding of whether aseismic slip is reducing the slip available for future seismic rupture beneath the Himalaya, we may reasonably reject an aseismic slip rate greater than 30% of the India/Tibet convergence rate. Thus aseismic slip, should it be occurring, at most reduces slip available for rupture causing an increase in the recurrence interval between great Himalayan earthquakes.

Our estimates for India/Tibet convergence of 9-18 mm/yr are consistent with independent estimates of this rate from geological and seismological estimates as well as with recent GPS measurements in Nepal. The leveling data suggest that horizontal deformation studies require a control point spacing of not less than 10 km if the mechanics of the collision process is not to be aliased by activity on the smaller-scale features we find to be currently active. Precise leveling data in southern Tibet are especially desirable to determine the mechanics of the inferred crustal scale ramp that is believed to be responsible for the recent uplift of the Greater Himalaya.

Acknowledgments. The leveling data were made available for this study by the Survey Department, Ministry for Housing and Land Development, His Majesty's Government of Nepal as part of a collaborative project with the University of Colorado to assess seismic hazard in the Nepal Himalaya. We thank M.R. Pandey for unpublished microseismic data and Devinath Subedi for his help with the Geology of the Siwalik Hills. We thank Wang Wenying for his help in processing the leveling data from Tibet. Special thanks to the Project INDEPTH team and K.D. Nelson for a preprint of their seismic results. Grant Marshal, Mike Ellis, Roland Bergman, and an anonymous reviewer greatly improved the manuscript. The Nepal seismic hazard study is funded by National Science Foundation grant EAR-8721163.

References

Avouac, J. P., and P. Tapponnier, Kinematic model of active deformation in central Asia, *Geophys. Res. Lett.*, *20*, 895-898, 1993.

Baranowski, J., J. Armbruster, L. Seeber and P. Molnar, Focal depths and fault plane solutions of earthquakes and active tectonics of the Himalaya, *J. Geophys. Res.*, *89*, 6918-6928, 1984.

Barrientos, S. E., R. S. Stein and S. N. Ward, Comparison of the 1959 Hebgen Lake, Montana and the 1983 Borah Peak, Idaho earthquakes from geodetic observations, *Bull. Seismol. Soc. Am.*, *77*, 784-808, 1987.

Bashyal, R. P., Exploration opportunities in Nepal, report, H.M.G. Dep. of Mines and Geol., Kathmandu, Nepal, 1990.

Bhattarai, D. R. Some geothermal springs of Nepal, *Tectonophysics, 62*, 7-11, 1980.

Bilham, R., Mountain metrology, *Appalachia*, *47* (187), 79-107, 1988.

Bilham, R., and G. C. P. King, The morphology of strike-slip faults: Examples from the San Andreas Fault, California, *J. Geophys. Res.*, *94*, 10,204-10,216, 1989.

Chen, W.P., and P. Molnar, Source parameters of earthquakes and intraplate deformation beneath the Shillong Plateau and northern Indoburman Ranges, *J. Geophys. Res.*, *95*, 12,527-12,552, 1990.

Copeland, P., and T. M. Harrison, Episodic rapid uplift in the Himalaya revealed by $^{40}Ar/^{39}Ar$ analysis of detrital K-feldspar and muscovite, Bengal fan, *Geology*, *18*, 354-357, 1990.

Delcaillau, B., Evolution morphostructurale d'un piédmont frontal de chaîne de collision intracontinentale: Les Siwaliks de l'Himalaya du Népal oriental, 435 pp., Univ. Toulouse le Mirail, , 1986.

DeMets, C., R. G. Gordon, D. F. Argus and S. Stein, Current plate motions, *Geophys. J. Int.*, *101*, 425-478, 1990.

Dickey, P. A., Who discovered Mount Everest?, *Eos Trans. 66 (41)*, 697-700, 1985.

Ellis, M. E., and G. C. P. King, Structural control of flank volcanism in continental rifts, *Science*, *254*, 839-842, 1991.

Gansser, A., The geodynamic history of the Himalaya, *in Zagros, Hindu Kush, Himalaya-Geodynamic Evolution*, Geodyn. Ser., vol. 5, edited by H. K. Gupta and F. M. Delaney, pp. 111-121, AGU, Washington, D.C., 1981.

Gomberg, J., and M. Ellis, Topography and tectonics of the central New Madrid seismic zone: Results of numerical experiments using a three-dimensional boundary element program, *J. Geophys. Res.*, this issue

Gu D., The determination of the height of Qomolangma Feng, *Sci.-Sin.*, XIX (2), 260-275, 1976.

Gulatee, B. L., The height of Mount Everest: A new differential determination (1952-54), *Tech. Pap. 8*, 23 pp., Surv. of India, Dehra Dun, 1954.

Harris, R., and P. Segall, Detection of a locked zone at depth on the Parkfield, California, segment of the San Andreas Fault, *J. Geophys. Res.*, *92*, 7945-7962, 1987.

Harrison, T. M, P. Copeland, W.S. F. Kidd, and An Yin, Raising Tibet, *Science*, *255*, 1663-1670, 1992.

Hirn, A., and M. Sapin, The Himalayan zone of crustal interaction: Suggestions from explosion seismology, *Ann. Geophys. 2*, 123-130, 1984.

Holdahl, S. R., A model of temperature stratification for correction of leveling refraction, *Bull. Geod.*, *55*, 239-249, 1981.

Iwata, S., Mode and rate of uplift of the Nepal Himalaya, *Z. Geomorphol.*, *63*, 37-49, 1987.

Iwata, S., T. Sharma, and H. Yamanaka, A preliminary report on geomorphology of central Nepal and Himalayan uplift, *J. Nepal Geol. Soc.*, *4*, 141-150, 1984.

Jackson, D. D., Interpretation of inaccurate, insufficient and inconsistent data, *Geophys. J. R. Astron. Soc.*, *28*, 97-109, 1972.

Jackson, M. and R. Bilham, Epoch GPS measurements across the Nepal Himalaya, *Geophys. Res. Lett., in press*, 1994.

Jackson, M., et al., Trans-Himalayan geodesy, *Eos Trans. AGU, 72* (44), Fall Meeting Suppl., 112, 1991.

Jackson, M., S. Barrientos, R. Bilham, B. Shrestha, and D. Kayestha, Uplift in the Nepal Himalaya revealed by spirit leveling, *Geophys. Res. Lett., 19*, 1539-1542, 1992.

Karukaranan, C., and A. Ranga Rao, Status of exploration for hydrocarbons in the Himalaya region, in Contributions to Stratigraphy and Structure, Himalayan Geology Seminar, Section III, Oil and Natural Gas Resources, Misc. Publ. 41, pp. 1-66, Geol. Surv. of India, New Delhi, India, 1979.

King, G. C. P., R. S. Stein, and J. B. Rundle, The growth of geologic structures by repeated earthquakes, 1, Conceptual framework, *J. Geophys. Res., 93*, 13,307-13,318, 1988.

Lanczos, C., Linear Differential Operators., Van Nostrand-Reinhold, Princeton, N. J., 1961.

Langbein, J. O., An interpretation of episodic creep on the Calavaris fault near Hollister, California, *J. Geophys. Res., 86*, 4941-4948, 1981.

Lawson, C. L., and D. J. Hanson, Solving Least Squares Problems. , Prentice-Hall, Englewood Cliffs, N. J., 1974.

Lépine, J. C., A. Hirn, M. R. Pandey, and J. M. Tater, Features of the *P*-waves propagated in the crust of the Himalayas, *Ann. Geophys., 2*, 119-121, 1984.

Lyon-Caen, H., and P. Molnar, Constraints on the structure of the Himalaya from an analysis of gravity anomalies and a flexural model of the lithosphere, *J. Geophys. Res., 88*, 8171-8191, 1983.

Lyon-Caen, H., and P. Molnar, Gravity anomalies, flexure of the Indian Plate, and the structure, support and evolution of the Himalaya and Ganga Basin, *Tectonics, 4*, 513-538, 1985.

Mason, K., Completion of the link connecting the triangulations of India and Russia, Rep. VI, Surv. of India, Delhi, India, 1914.

Mather, L. P. and G. Kohli, Exploration and development for oil in India, 6th World Petroleum Congress, Frankfurt and Main, Pr. Sec 1, 1964.

Menke, W., Geophysical Data Analysis: Discrete Inverse Theory, 289 pp., Academic, San Diego, Calif., 1989.

Milliman, J. D., and J. P. M. Syvitski, Geomorphic/tectonic control of sediment discharge to the ocean: The importance of small mountainous rivers, *J. Geol., 100*, 525-554, 1992.

Molnar, P., Inversion profiles of uplift rates for the geometry of dip-slip faults at depth, with examples from the Alps and the Himalaya, *Ann. Geophys., 5*, 663-670, 1987.

Molnar, P., A review of geophysical constraints on the deep structure of the Tibetan Plateau, the Himalaya, and the Karakoram and their tectonic implications, *Philos. Trans. R. Soc. London, Ser. A, 326*, 33-88, 1988.

Molnar, P., A review of the seismicity and rates of active underthrusting and deformation at the Himalaya, *J. Himalayan Geol., 1*, 131-154, 1990.

Molnar, P., and Deng Q., Faulting associated with large earthquakes and the average rate of deformation in Central and Eastern Asia, *J. Geophys. Res., 89*, 6203-6227, 1984.

Molnar, P., and P. Tapponnier, Cenozoic tectonics of Asia: Effects of a continental collision, *Science, 189*, 149-426, 1975.

Nakata, T., Active faults of the Himalaya of India and Nepal, *in* Tectonics of the Western Himalaya, edited by L. L. Malinconico and R. J. Lillie, *Spec. Pap. 232 Geol. Soc. Am.*, 243-264, 1989.

Nelson, K. D., Z. Wenjin, M. L. Hauck, L. D. Brown, M. Barazangi, and J. T. Kuo, First deep seismic reflection profile in the Himalaya/Tibet Plateau: Initial results of Project INDEPTH, *Eos Trans. AGU, 73* (43), Fall Meeting suppl., 544, 1992.

Ni, J., and M. Barazangi, Seismotectonics of the Himalayan collision zone: Geometry of the underthrusting Indian plate beneath the Himalaya, *J. Geophys. Res., 89*, 1147-1163, 1984.

Okada, Y., Surface deformation due to shear and tensile faults in a half-space., *Bull. Seismol. Soc. Am., 75*, 1135-1154, 1985.

Okada, Y., Internal deformation due to shear and tensile faults in a half-space, *Bull. Seismol. Soc. Am.*, 82, 1018-1040, 1992.

Pandey, M.R., and P. Molnar, The distribution of intensity of the Bihar-Nepal earthquake of 15 January, 1934 and bounds on the extent of the rupture zone, *J. Nepal Geol. Soc., 5*, 22-44, 1988.

Parker, R. L., Understanding inverse theory, *Annu. Rev. Earth Planet. Sci., 5*, 35-64, 1977.

Sastri, V.V., L.L. Bhandari, A.T.R. Raju, and A.K. Datta, Tectonic framework and subsurface stratigraphy of the Ganga basin, *J. Geol. Soc. India, 12*, 223-233, 1971.

Savage, J. C., W. H. Prescott, M. Lisowski, and N. E. King, Geodolite measurements of deformation near Hollister, California, 1971-1978, *J. Geophys. Res., 84*, 7599-7615, 1979.

Schelling, D., A balanced cross-section through the Eastern Nepal Siwalik Hills, Bagmati River region, implications for the structure of the southern Himalaya, *J. Nepal Geol. Soc., 8*, 1-10, 1992.

Schelling, D. and K. Arita, Thrust tectonics, crustal shortening, and the structure of the Far-Eastern Nepal Himalaya, *Tectonics, 10*, 851-862, 1991.

Seeber, L., and J. Armbruster, Great detachment earthquakes along the Himalayan arc and the long-term forecasts, in *Earthquake Prediction: An International Review*, Maurice Ewing Ser., vol. 4, edited by D. W. Simpson and P. G. Richards, pp. 259-277, AGU, Washington, D.C., 1981.

Seeber, L., J. Armbruster and R. Quittmeyer, Seismicity and continental subduction in the Himalayan arc, in *Zagros, Hindu Kush, Himalaya-Geodynamic Evolution, Geodyn. Ser.*, vol. 5, edited by H. K. Gupta and F. M. Delany, pp. 215-242, AGU, Washington, D.C., 1981.

Segall, P., and R. Harris, Slip deficit on the Parkfield, California, segment of the San Andreas fault as revealed by inversion of geodetic data, *Science, 233*, 1409-1413, 1986.

Shrestha, N. N., Leveling Instruction Book, Part 1, Field Work, HMG Nepal Survey Department, Geodetic Survey Branch, Kathmandu, Nepal, 1988.

Stein, R., G. C. P. King, and J. Lin, Change in failure stress on the southern San Andreas fault system caused by the 1992 magnitude=7.4 Landers earthquake, *Science, 258*, 1328-1332, 1992.

Stocklin, J., and K. D. Bhattarai, Geological map of Kathmandu area and central Mahabharat Range, scale 1:250,000, HMG Dept. of Mines and Geol., Kathmandu, Nepal, 1980.

Thatcher, W., Systematic inversion of geodetic data in central California, *J. Geophys. Res., 84*, 2283-2295, 1979.

Vasco, D. E., R. B. Smith and C. L. Taylor, Inversion for sources of crustal deformation and gravity change at the Yellowstone caldera, *J. Geophys. Res., 95*, 19,839-19,856, 1990.

Walpole, R. E., and R. H. Myers, Probability and Statistics for Engineers and Scientists, 639 pp., Macmillan, New York, 1985.

Wang, W., and Z. Yang, Application of the GPS technology in the survey of plate tectonic motion and vertical crustal displacement in the Himalaya area (in Chinese), *J. Xi'an Coll. Geol.*, 15, 1-8, 1993.

Ward, S. N., and S. E. Barrientos, An inversion for slip distribution and fault shape from geodetic observations of the 1983, Borah Peak, Idaho, earthquake, *J. Geophys. Res., 91*, 4909-4919, 1986.

Zeitler, P.K., Cooling history of the NW Himalaya, Pakistan, *Tectonics, 4*, 127-151, 1985.

Zhang Q., The problem of uplift rate of the Tibetan Plateau (in Chinese), Scientific Communication, in *Chinese Geodesy*, pp. 529-531, 1991, .

Zhao, W., et al., First deep seismic reflection profile on the Tibet Plateau: Initial results of Project INDEPTH, *Nature, 366*, 557-559, 1993.

R. Bilham and M. Jackson, CIRES, Campus Box 216, University of Colorado, Boulder, CO 80309. (e-mail: mikej@slip.colorado.edu)

(Received April 7, 1993; revised February 7, 1994; accepted March 14, 1994.)